Available online at www.sciencedirect.com

ScienceDirect

Procedia CIRP 85 (2019) 2–7

www.elsevier.com/locate/procedia

2nd CIRP Conference on Composite Material Parts Manufacturing (CIRP-CCMPM 2019)

Temperature field due to a moving heat source in machining orthotropic composites with arbitrary fiber orientation

Jan Mehnen*, Wolfgang Hintze, Lars Köttner, Robert von Wenserski

Institute of Production Management and Technology, Hamburg University of Technology, Denickestraße 17, Hamburg, Germany

Abstract

Milling of fiber reinforced plastics (FRP) is challenging with respect to surface integrity and tool wear due to high process temperatures. The maximum temperatures occurring in the workpiece determine the extent of the matrix decomposition area. Improving the workpiece quality therefore requires an understanding of its internal temperature distribution during milling. However, steep temperature gradients and high mechanical stress make measurements of temperature fields in the cutting zone difficult. In addition, thermal properties change depending on the fiber orientation in the case of orthotropic FRP.

In this paper, an existing model describing the temperature field for isotropic materials is extended to unidirectional, orthotropic FRP. Here, the thermal impact of an end mill upon the machined surface is represented by a strip-shaped heat source which moves with the feed velocity along a semi-infinite space. Starting with the temperature field of an instantaneous point source, multiple integration steps and a coordinate transformation lead to the temperature field of the moving strip source for orthotropic materials with arbitrary fiber orientation.

Using this analytical approach, two-dimensional temperature fields within the workpiece can be calculated for various feed velocities, heat source widths and fiber orientation angles. A cross verification of the analytical solution is successfully carried out by comparing it to a numerical simulation. Furthermore, temperature measurements during end milling of carbon fiber reinforced plastics using thermocouples confirm these results for different fiber orientations.

The derived model can be applied to a variety of heat flow problems relevant for orthotropic materials, e.g. other machining technologies.

Peer-review under responsibility of the scientific committee of the 2nd CIRP Conference on Composite Material Parts Manufacturing.

Keywords: Composite; Temperature; Modeling; Milling; Orthotropic

1. Introduction

Fiber reinforced plastics (FRP), and in particular carbon fiber reinforced plastics (CFRP), are increasingly used in high-perfomance environments such as the aerospace industry for their remarkable specific strength, corrosion resistance and adjustable directional properties. Consequently, modern aircraft feature high FRP contents, e.g. Airbus A350 with 53 wt.-% CFRP [1] and Boeing 787 with 50 wt.-% FRP [2].

For ideal utilization of the mechanical properties of CFRP in structural components such as aircraft wings, a unidirectional (UD) fiber-layout with high fiber volume content is used. After primary near-net shaping, the components are usually finished by machining the contour, whose length may amount to several dozen meters. For this step, milling is one of the most commonly used processes [3]. As most of the part's added value is generated beforehand, high quality and reliability are demanded of FRP machining processes which are especially challenging due to anisotropic behavior as well as low thermal resistance of the matrix and abrasiveness of the fibers.

Mechanical damages from machining CFRP, such as delamination, have shown themselves to be highly dependent on the fiber orientation angle Φ between surface ply fibers and feed direction (defined in Fig. 4), as shown by [4, 5, 6]. In addition, the cutting forces are associated with the fiber orientation, with $\Phi = 0°$ showing the lowest and $\Phi = 90°$ the highest forces [7].

Thermal damages in the workpiece result from overheating of the matrix in the so-called heat-affected zone (HAZ) at the machined edge. Here, in the temperature range between glass transition temperature T_g and the point of pyrolysis, the matrix stiffness drops rapidly [8, 9, 10]. Consequently, when the temperatures in the vicinity of the tool exceed T_g, the matrix cannot sufficiently support the carbon fibers, leading to poor machin-

* Corresponding author. Tel.: +49-40-42878-3403 ; fax: +49-40-4273-14554.

E-mail address: jan.mehnen@tuhh.de (Jan Mehnen).

2212-8271
Peer-review under responsibility of the scientific committee of the 2nd CIRP Conference on Composite Material Parts Manufacturing.
10.1016/j.procir.2019.09.019

ing quality [11]. For UD-workpieces with orthotropic or rather transversely isotropic thermal properties, the generated temperatures depend on the fiber orientation. Maximum temperatures are low for $\Phi = 45°$ and high for $\Phi = 135°$ as shown by Wang et al. [12] for UD-CFRP as heat conduction from the cutting zone into the workpiece is amplified when the fibers are aligned with the temperature gradient.

The temperature field may be calculated by numerical simulation of a heat source (representing the tool) moving at the machined edge of an orthotropic body, as shown by Mkaddem et al. for a UD glass fiber reinforced plastic workpiece [13]. Sheikh-Ahmad et al. used a similar approach for a plain-weave CFRP workpiece with equal conductivities in planar direction and lower conductivity perpendicular to the workpiece surface while also considering heat loss by convection in their simulation [14]. These numerical simulations show comparatively long computation times due to the necessary approach of a steady-state as well as fine discretization of time and space in the area of steep temperature gradients.

This paper establishes an analytical model for the temperature field due to a heat source moving at the machined edge of an orthotropic workpiece with arbitrary fiber orientation, based on an approach for isotropic material developed by Jaeger [15]. The model is cross-verified by comparison to a numerical simulation and experimentally validated by thermocouple temperature measurements in a steady-state UD-CFRP milling process.

2. Analytical model of the temperature field

Machining is a complex thermomechanical interaction of tool cutting edge and workpiece material. The anisotropic properties of FRP complicate the description of occurring phenomena even more due to the high number of fibers in the material being cut as well as the directional heat properties. As the scope of the presented model is to exclusively describe the temperature field within the workpiece that is inflicted by the cutting process, several simplifications are made. First of all, there is no consideration of cutting and chip removal, i.e. no mechanical calculations are made. Furthermore, the heating of the workpiece due to the temperature of chips and tool is replaced by a strip-shaped heat source with constant heat flux, disregarding the actual periodic heat flux due to discontinuous cutting. The heat source representing the tool moves along the confining wall of a semi-infinite solid which is otherwise adiabatic, as shown in Fig. 1. Consequently, the problem is regarded as two-dimensional as there is no heat conduction in y-direction. Finally, the material properties are constant, making them temperature-independent.

In the following derivation, the general description of the problem and the boundary conditions (BCs) are illustrated by example of the existing model for isotropic bodies. For orthotropic solids, one of the mutually perpendicular conductivities of heat is parallel to the y-axis of Fig. 1 while the other two are rotated around the y-axis by coordinate transformation.

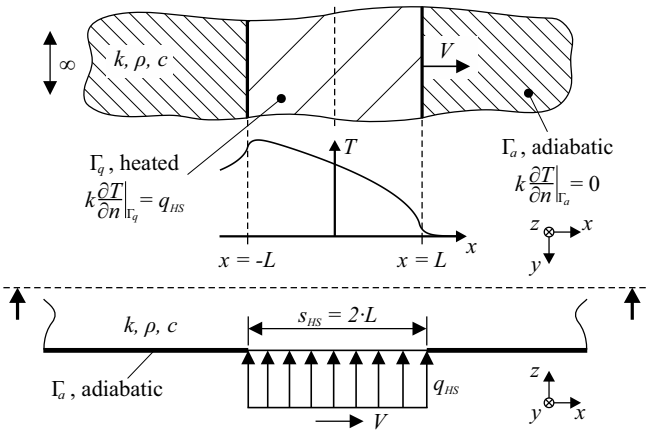

Fig. 1. Model of semi-infinite wall for analytical approach

2.1. Temperature field for isotropic bodies

Calculations for the estimation of machining process temperatures exist for isotropic workpiece materials on the basis of the moving strip source which builds on the partial differential equation of heat conduction for isotropic solids in Eq. (1).

$$\frac{\partial^2 T}{\partial x^2} + \frac{\partial^2 T}{\partial y^2} + \frac{\partial^2 T}{\partial z^2} = \frac{\rho c}{k}\frac{\partial T}{\partial t} \tag{1}$$

Eq. (1) is satisfied for the infinite solid by the instantaneous point source (IPS) of strength Q at position $P' = (x', y', z')$ in Eq. (2), whereas the IPS is located at $P' = (0, 0, 0)$ for usability.

$$T_{\mathrm{IPS,I}} = \frac{Q\,(\rho c)^{1/2}}{8\,(\pi\,k\,t)^{3/2}} \mathrm{e}^{-\frac{\rho c}{4kt}\left[(x-x')^2+(y-y')^2+(z-z')^2\right]} \tag{2}$$

The temperature change $T_{\mathrm{IPS,I}}$ is calculated at the location of interest $P = (x, y, z)$ for a point in time $t > 0$ after the initial liberation of heat. The index I identifies the isotropic body. ρ, c and k denote the material density, the heat capacity and the heat conductivity. Eq. (2) is a Green's function, whose derivation can be found in [16].

For the temperature field due to a moving strip source, Eq. (2) is adapted to a semi-infinite solid and subjected to several consecutive integration steps. In this process, a general domain Ω with initial temperature T_0 and boundary Γ, consisting of the heated area Γ_q and the adiabatic area Γ_a, is assumed:

$$k\frac{\partial T}{\partial n}\bigg|_{\Gamma_q} = q_{HS}, \quad k\frac{\partial T}{\partial n}\bigg|_{\Gamma_a} = 0, \quad T(x, y, z, t = 0) = T_0, \tag{3}$$

Here, the BCs describe the applied constant heat flux q_{HS} on the heated surface and the disabled heat flux on the adiabatic

surfaces, see Fig. 1. The initial condition describes the constant temperature in the whole domain at time $t = 0$.
Using Eq. (2), a formulation for the temperature field due to a moving strip source (MSS) with velocity V is derived, see Eq. (4). A detailed description of its derivation was given by Jaeger [15] and comprehensively by Carslaw and Jaeger [17].

$$T_{\mathrm{MSS,I,SS}} = \frac{q_{HS}}{\pi k} \int_{x-L}^{x+L} \mathrm{e}^{-\frac{\rho c V S}{2k}} K_0 \left\{ \frac{\rho c V \sqrt{S^2 + z^2}}{2k} \right\} \mathrm{d}S \qquad (4)$$

Here, $K_0\{\}$ denotes the modified Bessel function of the second kind of order zero. The integration variable $S = x - x'$ is introduced for better readability. The index SS identifies the steady state of $t \to \infty$.

2.2. Derivation of temperature field for orthotropic bodies

A similar approach to section 2.1 was used for the orthotropic body. It is based on the partial differential equation of heat conduction for orthotropic solids in Eq. (5).

$$k_{11} \frac{\partial^2 T}{\partial x^2} + k_{22} \frac{\partial^2 T}{\partial y^2} + k_{33} \frac{\partial^2 T}{\partial z^2} = \rho c \frac{\partial T}{\partial t} \qquad (5)$$

Orthotropic heat conduction in Eq. (5) demands that the formulation for the IPS in isotropic materials from Eq. (2) is adapted to Eq. (6), see Carslaw and Jaeger [17].

$$T_{\mathrm{IPS,O}} = \frac{Q(\rho c)^{1/2}}{8(\pi^3 t^3 k_{11} k_{22} k_{33})^{1/2}} \exp\left(-\frac{\rho c}{4t} \left[\frac{(x-x')^2}{k_{11}} + \frac{(y-y')^2}{k_{22}} + \frac{(z-z')^2}{k_{33}} \right] \right) \qquad (6)$$

Eq. (6) describes the instantaneous point source for orthotropic materials. Here, k_{11} denotes the heat conductivity parallel to the fiber direction x, whereas k_{22} and k_{33} refer to the conductivities perpendicular to the fiber direction, corresponding to y and z.

Following the process described in Fig. 2, the formulation of the MSS follows with Eq. (7). Except for the previously used isotropic heat conductivity k, the same BCs and initial condition as described in section 2.1 and shown in Fig. 1 apply. A coordinate transformation around the y-axis through the fiber orientation angle Φ yields the new coordinate system x_n, y_n, z_n.

Again, the integration variable S is introduced for better readability. The index Φ implies that an arbitrary fiber orientation of the orthotropic body may be used in the calculation. The conductivities of heat k_{11} and k_{33} are therefore not parallel to the coordinate axes x_n and z_n for $\Phi \neq 0°$ after the coordinate transformation in step two of Fig. 2. For $k_{11} = k_{33}$, Eq. (7)

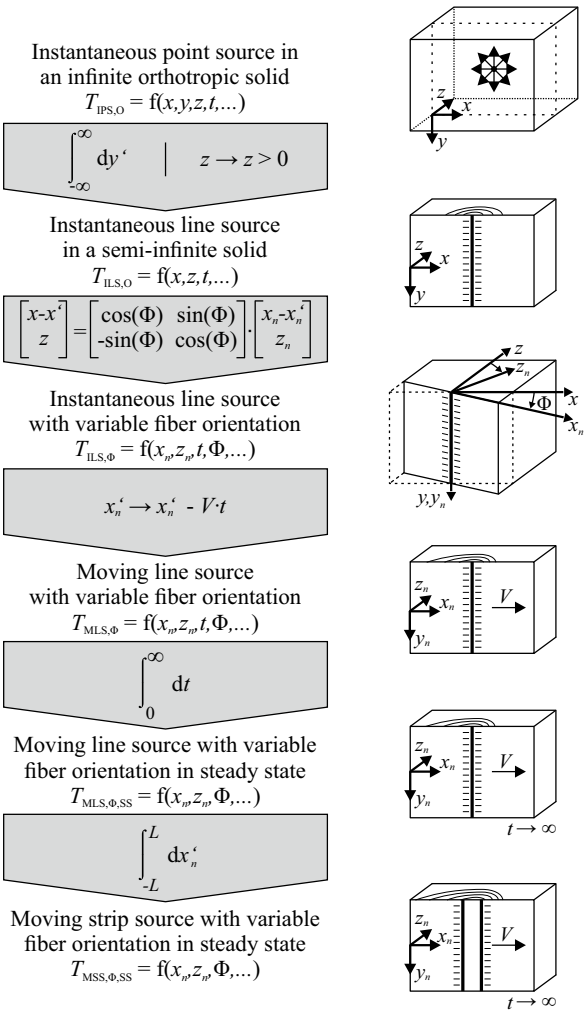

Fig. 2. Derivation of the orthotropic moving strip source

naturally leads to Eq. (4).

$$T_{\mathrm{MSS,\Phi,SS}} = \frac{q_{HS}}{\pi \sqrt{k_{11} k_{33}}} \int_{x_n-L}^{x_n+L} \exp\left(\frac{\rho c V}{2k_{11}k_{33}} \left[(k_{11} - k_{33})(S \cos^2 \Phi + z_n \sin \Phi \cos \Phi) - k_{11} S \right] \right) K_0 \left\{ \frac{\rho c V}{2k_{11}k_{33}} \left(k_{11} - (k_{11} - k_{33}) \cos^2 \Phi \right)^{1/2} \left[\left(k_{11} - k_{33} \right) \left((z_n^2 - S^2) \cos^2 \Phi - 2 z_n S \sin \Phi \cos \Phi \right) + k_{11} S^2 + k_{33} z_n^2 \right]^{1/2} \right\} \mathrm{d}S \qquad (7)$$

2.3. Model verification through numerical simulation

To verify the derived formulation in Eq. (7), its results for the maximum surface temperature change were compared to those of a numerical simulation with input parameters shown in Fig. 3 and fiber orientation steps of $\Delta\Phi = 5°$. For the simulation,

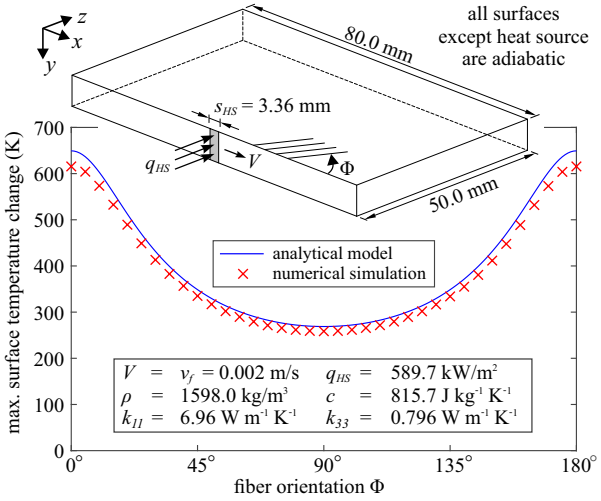

Fig. 3. Setup of numerical simulation and comparison with analytical model

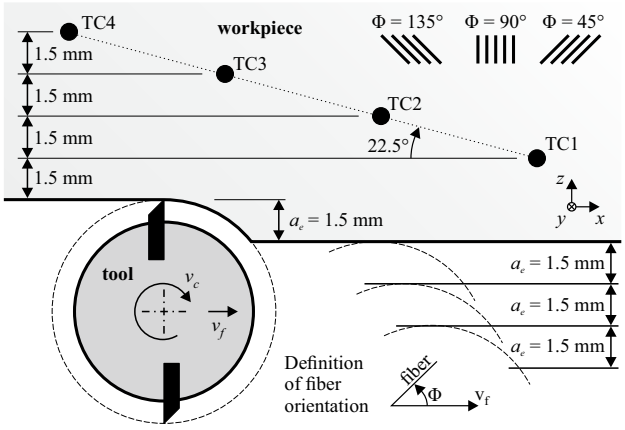

Fig. 4. Experimental setup at the last of four cuts

ABAQUS/Standard was used with the user-subroutine DFLUX representing the moving heat source. To achieve a good approximation at reasonable computation times, a mesh of 9110 nodes and 6832 elements of type DC3D6 (6-node linear heat transfer triangular prism) and a time step of 0.05 s were used. The maximum element size on the heated edge was 0.025 mm, made necessary by steep temperature gradients there. Biased seeding up to a size of 10 mm at the back edge was used. The general setup of the numerical simulation and its comparison to the results of the analytical model of Eq. (7) is shown in Fig. 3. Small deviations from the analytical model result from the granularity of mesh sizes and time steps.

This comparison cross-verifies model and simulation and enables using the model as a benchmark for other simulations.

3. Experimental approach

For experimental validation of the analytical model, milling experiments were conducted on UD-CFRP panels with varying fiber orientation. Thermocouples (TCs) were used to measure the temperature in four distances from the cutting edge. Four consecutive cuts in the same vertical distance as the TCs were conducted for each fiber orientation to gain redundancy, Fig. 4.

3.1. Material and tool

UD-CFRP panels made of Cycom 977-2-35-24K IMS 268 prepregs with 268 gsm were used. The 0.25 mm thick layers in a $[0]_{16}$ layup led to a workpiece thickness of 4.0 mm. Curing was done according to the data sheet in [18]. Thermal properties of the panels are shown in Table 1 and were taken as room temperature properties of Cytec IM7/977-2/UD from Joven et al. [19]. Material density was calculated by adding the densities of epoxy matrix [18] and carbon fibers [20], according to the fiber volume content of 65 %.

A PCD-tipped two-fluted end mill [*Gühring KG*] was used on a machining center Röders RFM600 [*Röders GmbH*]. Tool properties are shown in Table 2.

Table 1. Material properties of CFRP workpiece used for milling experiments

Parameter	Symbol	Value	Unit
Density	ρ	1598	kg/m^3
Specific heat	c	815.7	J kg^{-1}K^{-1}
Heat conductivity parallel to fibers	k_{11}	6.96	W m^{-1}K^{-1}
Heat conductivity perpendicular to fibers	k_{33}	0.796	W m^{-1}K^{-1}

Table 2. Tool properties and machining parameters of milling experiments

Parameter	Symbol	Value	Unit
Cutting speed	v_c	100	m/min
Feed per tooth	f_z	0.015	mm
Feed rate	v_f	0.002	m/s
Tool engagement (radial depth of cut)	a_e	1.5	mm
Depth of cut (workpiece thickness)	a_p	4.0	mm
Tool diameter	d_t	8.0	mm
Clearance angle	α_f	12	°
Rake angle	γ_f	0	°
Helix angle	δ	1.6	°

3.2. Process parameters and measurement equipment

Process parameters were set according to Table 2. Fiber orientation angles of $\Phi = 45°$, 90° and 135° were experimentally investigated. A fiber orientation of $\Phi = 0°$ was not realized due to workpiece splitting in feed direction at radial depth of cut a_e.

For temperature measurements, four Type-J TCs (TC1 to TC4) of Tolerance Class 1 with stainless steel sheaths of Ø 0.5 mm were used [*TC GmbH*]. Blind holes of Ø 0.6 mm and 2.1 mm depth were drilled into which the TCs were inserted after being filled with heat conductive paste. The small diameter presumably led to almost no disturbance of the heat flow but should be further investigated. The TC placement at an angle of 22.5° as shown in Fig. 4 such that the TCs were not ever aligned with the fibers minimized the temperature field disturbance.

TC measurements were conducted using an input module NI 9210 [*National Instruments Corp.*] which limited the overall sample rate to 14 Hz. Using four TCs led to a sample rate of 3.5 Hz. The feed rate v_f was chosen to be comparatively small

so that the limited sample rate still enabled a sufficiently accurate mapping of temperature change with reference to RT (one sample was taken after every 0.57 mm of feed movement).

TC1 was placed on the panel so that it was aligned with the tool after a feed path of 200 mm. The assumed steady-state at this position was confirmed by sideways thermal imaging with an infrared camera thermoIMAGER TIM 400 [*Micro-Epsilon GmbH*], comparable to the setup in [14]. Here, an equilibrium of tool and chuck temperature was observed.

For the spindle power, torque was measured by a rotating dynamometer 9123C [*Kistler Instrumente AG*] and multiplied by the tool's angular velocity. The average mechanical power was then determined to be 27.41 W for $\Phi = 45°$, 38.56 W for $\Phi = 90°$ and 36.55 W for $\Phi = 135°$.

3.3. Model fitting to experimental results

The analytical model in Eq. (7) was fitted to the experimental average maximum temperatures for each vertical distance (see redundancy in section 3) with MATLAB's built-in function *lsqnonlin()*. In the presence of parameter boundaries, this function solves nonlinear least-squares problems using the *Trust-Region-Reflective Least Squares Algorithm*, where the actual error function is approximated by a simpler function within so-called trust regions around the current point, see [21]. The algorithm estimated the heat source's thermal contact length $s_{HS} = 2L$ and heat flux q_{HS} so that the sum of squared errors between measured maximum temperatures and modeled temperatures reaches a minimum. This best fit is depicted in Fig. 5.

For a known T_g (such as e.g. $T_g = 170°C$ of the used matrix system [18]), the HAZ depth is evident in this diagram. Values for s_{HS}, q_{HS} and the estimated maximum surface temperature $\Delta T_{S,max}$ are given in Fig. 6. The thermal contact length s_{HS} represents the dimension effective for heat transfer into the workpiece rather than a geometrical quantity and varies significantly with Φ. Alignment of fibers to heat gradient is decisive for the heat conduction into the workpiece, confirming the results of Wang et al. [12] for the "dissipation region". The heat flow P_{HS} is calculated by multiplying q_{HS} with s_{HS} and the experimental material thickness of 4.0 mm. The percentages in Fig. 6 refer to the ratio of heat flow to spindle power, calculated using the values from section 3.2.

Further confirmation of the fitting is achieved by comparison of temperature developments over x-coordinate of both experiment and fitted model in Fig. 7 (the measurements of the TCs were taken from the last cut for each fiber orientation, see Fig. 4). Here, cooling effects become obvious, as the fitted model continuously shows higher temperatures than the experiment behind the peak temperature (in negative x-direction, equivalent to a later measurement). For $\Phi = 45°$ and $\Phi = 135°$, the measured peak temperatures of TC3 and TC4 show higher values than the model, suggesting that the actual heat flow is even higher. A possible explanation is a cut-off at the peak temperature of TC1 due to the limited dynamic behavior of the TC.

Finally, the estimated values for thermal contact length and heat flow were used to plot temperature fields for the different fiber orientations, see Fig. 8.

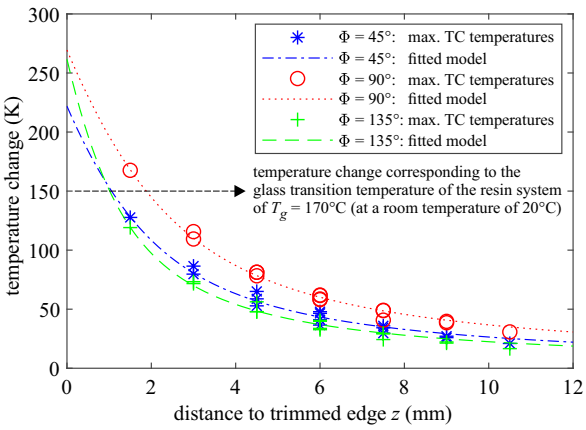

Fig. 5. Fitting of model to maximum measured TC temperatures

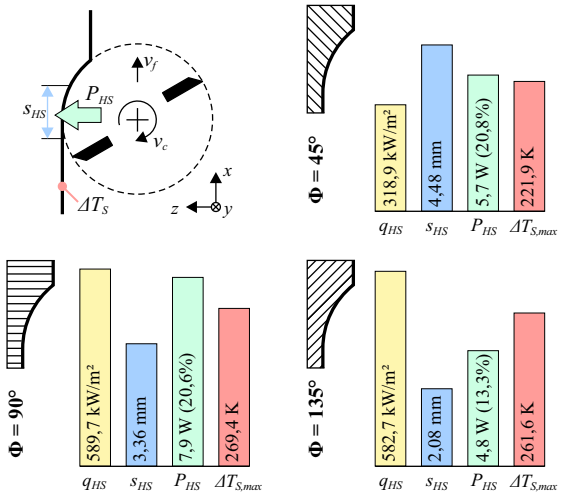

Fig. 6. Results of model fitting to TC measurements - for realistic numbers, values of $\Phi = 90°$ were used for the numerical simulation in Fig. 3

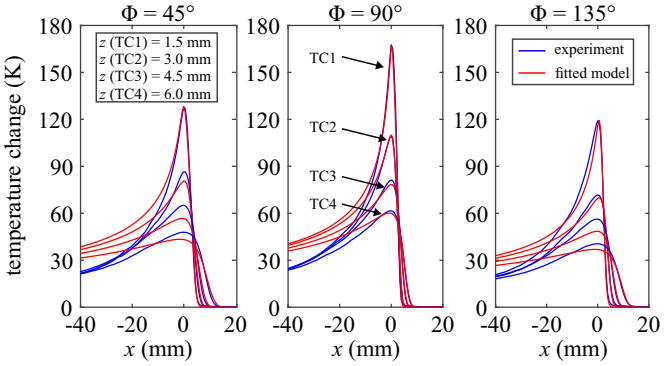

Fig. 7. TC temperature measurements and fitted model at last cut over x-coordinate (temperature curves were aligned with the peak at $x = 0$ mm)

4. Summary and outlook

An analytical model for the calculation of temperature fields within orthotropic bodies with variable fiber orientation subjected to a moving heat source was derived. The model was successfully cross-verified with a numerical simulation by compar-

ing the maximum surface temperatures in steady-state. Fitting the model to the results of milling experiments shows that the estimated heat flow and the estimated thermal contact length strongly depend on the fiber orientation angle Φ. The comparison of model and experiment revealed a ratio of heat flow to spindle power between 13.3 and 20.8%, also depending on the fiber orientation angle. This ratio is expected to be a function of tool diameter, process parameters and involved material combinations of tool and workpiece. Considering the maximum extension of the isotherms corresponding to the critical temperature T_g of the resin, the maximum depth of the HAZ occurs at Φ = 90°, and the minimum at Φ = 135°, see also Fig. 5. Comparing Fig. 6 and Fig. 8, it can be concluded that the maximum temperature change at the surface $\Delta T_{S,max}$ doesn't indicate the extent of the HAZ. Only when considering all parameters (including Φ) is it possible to estimate the temperature field.

For the experiments, tool temperature measurements as demonstrated by Kerrigan et al. in [22] could be implemented to confirm steady-state and to estimate the temperature field in combination with the known process and material parameters.

The standard shape of the heat source strength as shown in Fig. 1 is rectangular. Additional research should investigate different shapes, as discussed among others by Jaeger [15] for heat sources with a strength of triangular or parabolic shape.

Furthermore, the heat conduction properties, which were assumed to be constant, are actually temperature-dependent as shown by Joven et al. [19] and could be implemented as such.

Also, convectional surface cooling could be included, similar to the approach by DesRuisseaux and Zerkle [23].

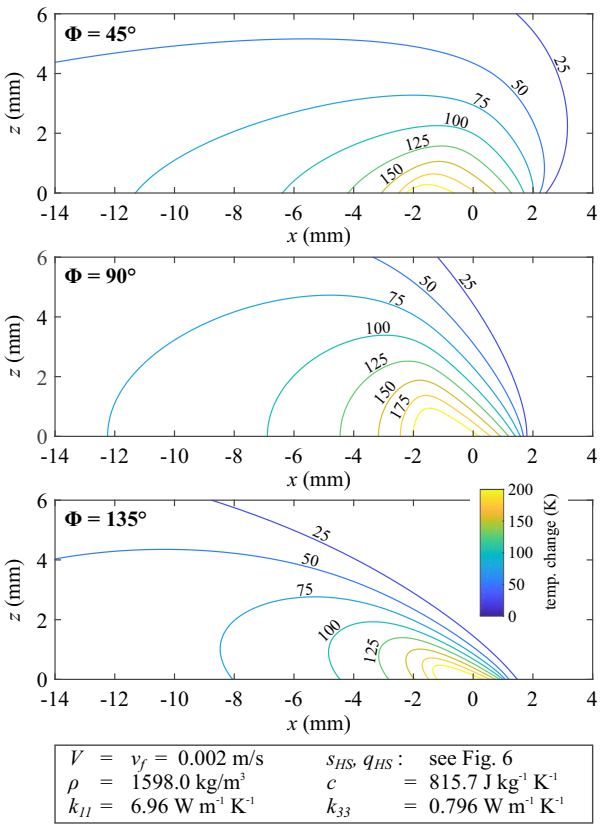

Fig. 8. Temperature fields ΔT for the different fiber orientations

Acknowledgements

The authors would like to cordially thank *Gühring KG* for the provision of PCD-tools.

References

[1] Airbus SE, "Airbus technical magazine - FAST: Special Edition A350XWB," 2013.
[2] The Boeing Company, "AERO: QTR_04," 2006.
[3] J. Y. Sheikh-Ahmad, *Machining of Polymer Composites*. Boston, MA: Springer US, 2009.
[4] A. Koplev, A. Lystrup, and T. Vorm, "The cutting process, chips, and cutting forces in machining CFRP," *Composites*, vol. 14, no. 4, 1983.
[5] K. Colligan and Ramulu M, "The effect of edge trimming on composite surface plies," *Manufacturing Review*, vol. 5, no. 5, pp. 274–283, 1992.
[6] W. Hintze, D. Hartmann, and C. Schütte, "Occurrence and propagation of delamination during the machining of carbon fibre reinforced plastics (CFRPs)," *Composites Sc. and Tech.*, vol. 71, no. 15, pp. 1685–1790, 2011.
[7] D. H. Wang, M. Ramulu, and D. Arola, "Orthogonal cutting mechanisms of graphite/epoxy composite. Part I: unidirectional laminate," *Int. J. of Machine Tools and Manufacture*, vol. 35, no. 12, pp. 1623–1638, 1995.
[8] K. Kerrigan and G. E. O'Donnell, "On the relationship between cutting temperature and workpiece polymer degradation during CFRP edge trimming," *Procedia CIRP*, vol. 55, pp. 170–175, 2016.
[9] A. Chatterjee, "Thermal degradation analysis of thermoset resins," *Journal of Applied Polymer Science*, vol. 114, no. 3, pp. 1417–1425, 2009.
[10] F. C. Campbell, *Structural Composite Materials*. Materials Park, Ohio: ASM International, 2010.
[11] H. Wang, J. Sun, J. Li, L. Lu, and N. Li, "Evaluation of cutting force and cutting temperature in milling carbon fiber-reinforced polymer composites," *The Int. J. of Adv. Manufacturing Tech.*, no. 82, pp. 1517–1525, 2016.
[12] H. Wang, J. Sun, D. Zhang, K. Guo, and J. Li, "The effect of cutting temperature in milling of carbon fiber reinforced polymer composites," *Composites Part A: Applied Science and Manuf.*, vol. 91, pp. 380–387, 2016.
[13] A. Mkaddem, M. Zain-ul Abdein, S. Mezlini, A. S. Bin Mahfouz, and A. Jarraya, "Sensitivity of GFRP Composite Integrity to Machining-Induced Heat: A Numerical Approach," vol. 5 of *Applied Condition Monitoring*, pp. 205–214, Springer Int. Pub., 2017.
[14] J. Y. Sheikh-Ahmad, F. Almaskari, and F. Hafeez, "Thermal aspects in machining CFRPs: effect of cutter type and cutting parameters," *The Int. J. of Adv. Manufacturing Tech.*, vol. 302, no. 9–12, p. 1113, 2018.
[15] J. C. Jaeger, "Moving sources of heat and the temperature at sliding contacts," *J. and Proc. of the Royal Soc. of NSW*, vol. 76, pp. 203–224, 1942.
[16] K. Cole, J. Beck, A. Haji-Sheikh, and B. Litkouhi, *Heat Conduction Using Green's Functions*. CRC Press, 2 ed., 2010.
[17] H. S. Carslaw and J. C. Jaeger, *Conduction of Heat in Solids*. Oxford: Clarendon Press, 2. ed., 1959.
[18] Solvay S.A., "Technical Data Sheet CYCOM 977-2 and 977-2A," 2018.
[19] R. Joven, R. Das, A. Ahmed, P. Roozbehjavan, and B. Minaie, "Thermal properties of carbon fiber-epoxy composites with different fabric weaves," *Proceedings of SAMPE Tech*, vol. 2012, 2012.
[20] Teijin Limited, "Tenax filament yarn - product data sheet (EU)," 2018.
[21] R. H. Byrd, R. B. Schnabel, and G. A. Shultz, "Approximate solution of the trust region problem by minimization over two-dimensional subspaces," *Mathematical Programming*, vol. 40-40, no. 1-3, pp. 247–263, 1988.
[22] K. Kerrigan and G. E. O'Donnell, "Temperature Measurement in CFRP Milling Using a Wireless Tool-Integrated Process Monitoring Sensor," *Int. J. of Automation Tech.*, vol. 7, no. 6, pp. 742–750, 2013.
[23] N. R. DesRuisseaux and R. D. Zerkle, "Temperature in semi-infinite and cylindrical bodies subjected to moving heat sources and surface cooling," *Journal of Heat Transfer*, vol. 92, no. 3, p. 456, 1970.